

PCCP

Accepted Manuscript



This is an *Accepted Manuscript*, which has been through the Royal Society of Chemistry peer review process and has been accepted for publication.

Accepted Manuscripts are published online shortly after acceptance, before technical editing, formatting and proof reading. Using this free service, authors can make their results available to the community, in citable form, before we publish the edited article. We will replace this *Accepted Manuscript* with the edited and formatted *Advance Article* as soon as it is available.

You can find more information about *Accepted Manuscripts* in the [Information for Authors](#).

Please note that technical editing may introduce minor changes to the text and/or graphics, which may alter content. The journal's standard [Terms & Conditions](#) and the [Ethical guidelines](#) still apply. In no event shall the Royal Society of Chemistry be held responsible for any errors or omissions in this *Accepted Manuscript* or any consequences arising from the use of any information it contains.

Intramolecular vibrational redistribution in the non-radiative excited state decay of uracil in the gas phase: an ab initio molecular dynamics study

Philippe Carbonniere,^{1,*} Claude Pouchan,¹ Roberto Improta^{2,*}

March 30, 2015

1) Université de Pau et des Pays de l'Adour UMR5254 - IPREM - Equipe Chimie-Physique HélioParc - 2 av. Président Angot 64053 Pau Cedex 09

2) CNR–Consiglio Nazionale delle Ricerche, Istituto di Biostrutture Biommagini (IBB-CNR) Via Mezzocannone 16, I-80136, Napoli, Italy.

e-mail:philippe.carbonniere@univ-pau.fr,robimp@unina.it

Abstract

We report a study of the intramolecular vibrational distribution (IVR) occurring in the ground electronic state of Uracil (S_0) in the gas phase, following photoexcitation on the lowest energy bright excited state ($S\pi$) and decay through the ethylene-like $S\pi/S_0$ Conical Intersection ($CI-0\pi$). To this aim we have performed 20 independent Ab Initio Molecular Dynamics starting from $CI-0\pi$ (ten of them with 1 eV of kinetic energy randomly distributed over the different molecular degrees of freedom) and 10 starting from the ground state minimum (Franck-Condon, FC, point), with an excess kinetic energy equal to the energy gap between $CI-0\pi$ and the FC point. The simulations, exploiting PBE0/6-31G(d) calculations, were performed over an overall period of 10 ps. A thorough statistical analysis of the the variation of the geometrical parameters of Uracil during the simulation time and of the distribution of the kinetic energy among the different vibrational degrees of freedom provides a consistent picture of the IVR process. In the first 0-200 fs the structural dynamics involve mainly the recovery of the average planarity. In the 200-600 fs time range, a substantial activation of CO and NH degrees of freedom is observed. After 500~600 fs most of the geometrical parameters reach average values similar to those found after 10 ps, though the system cannot yet be considered in equilibrium.

1 Introduction

Vibrational cooling (VC) is a fundamental process for photochemistry and photophysics.¹⁻⁷ Following absorption of light, an excess of vibrational energy is deposited in a molecule and is redistributed among the different molecular vibrational levels (Intramolecular Vibrational Redistribution, IVR)^{1-yamada} before it is finally dissipated to the environment, usually the surrounding solvent molecules, until thermal equilibrium is re-established.

For what concerns intramolecular processes, the study of the IVR mechanism in the gas phase has attracted significant attention,⁸⁻¹⁹ since it is ubiquitously involved in physical, chemical and biological processes. An atomistic understanding of the formation and the breaking of bonds, a process lying at the heart of chemistry, requires indeed a full comprehension of vibrational energy redistribution.⁸⁻¹² In the last decades the processes governing the energy flow between the different molecular vibrational degrees of freedom have been thoroughly studied both experimentally and theoretically, such that an exhaustive review of the contributions in this field is now far beyond the scope of any short introduction. Instead we refer to a few fundamental works.⁸⁻¹⁵ From the experimental point of view, the developments in High resolution IR spectroscopy⁹, 2D-IR spectroscopy (see¹⁰ and references therein) and in multi photon photo-electron spectroscopy¹² have provided fundamental insights on the interplay between a bright spectroscopic state (which is 'prepared' following light absorption) and dark ones, which are coupled to the former via anharmonic couplings. The possibility of controlling the course of a chemical reaction by selectively exciting different molecular vibrational modes is a spectacular proof of the importance of exact knowledge of the involved IVR.¹¹ Conversely, theoretical approaches, despite the success of purely statistical theory as the RRKM theory,¹³ have successfully sought for more refined models able, for example, to understand mode-specific processes.^{14,15}

In the present contribution we shall focus on a case seldom tackled by theoretical approaches, i.e. that of a photoexcited molecule at a conical in-

tersection between an excited and the ground (S_0) electronic state. Once the Wave-Packet (WP) has decayed to S_0 , on the molecule there is a considerable amount of energy (of the order of some eV) that has to be thermalized and, in the meantime, affects its spectral properties. The absorption spectra of vibrationally hot molecules are indeed red-shifted with respect to their equilibrium counterpart and VC is mirrored by a blue-shift of the transient spectra.^{20–28}

The VC rates span a rather wide time range, between few ps and some tenths of ps, and strongly depend on the solvent, being larger for hydrogen bonding solvents. Its study can thus give fundamental insights on solute-solvent interaction and on energy transfer in complex systems. Furthermore, the VC rate can directly affect the photophysical and photochemical reactivity: until the energy is not dissipated it is available for further reactions, potentially being even more important than excited state reactivity, as proposed for the formation of pyrimidine photohydrates.²⁹ Finally, VC processes can make the assignment and the interpretation of the experimental time-resolved spectra more cumbersome.

Despite its importance, and the important insights obtained by using phenomenological models,^{24,25} microscopic mechanisms at the base of VC processes are still elusive and the number of studies on this topic rather limited, while several experimental results have been recently reported in the literature.^{20–25}

In an interesting study of 9-methyl-Adenine in different solvents, Middleton et al. have shown that the VC rate, besides depending, as expected, on the hydrogen bonding (HB) properties of the solvent, is different in water and in D_2O .²¹ Solvent isotope effect may indicate that a considerable portion of the excess energy decays by exciting relatively high frequency ($>700\text{ cm}^{-1}$) solvent modes. Not only low-frequency modes, which can be considered as friction, are thus involved in the solute-solvent vibrational energy transfer, but specific solute vibrations, requiring a more accurate treatment. This conclusion is supported by very recent studies on purine derivatives²⁰ and on VC in photoexcited thymine.^{24,25} The insensitiveness of the VC rate to temperature changes

can be explained by invoking the involvement of high frequency modes in the solute, which directly transfer vibrational quanta to solvent modes with the same frequency.²⁵

It is clear that these experimental results can be explained only by monitoring the intramolecular and intermolecular energy transfer processes at an atomistic level. As a first step in this direction, we here report a study of IVR in the ground electronic state of Uracil (hereafter Ura) in the gas phase, following photoexcitation in the UV. In particular we shall study, by using Ab Initio Molecular Dynamics simulations, the processes occurring in a hot Ura molecule soon after the lowest energy $\pi\pi^*$ bright excited state has non radiatively decayed to S_0 , via a Conical Intersection, in the absence of external interactions. This is a process where a substantial amount of potential energy is deposited on our system (for nucleobases, see also below, typically ~ 4.0 eV), that is very far from equilibrium, particularly suitable to be treated by atomistic calculations. Many of the other theoretical models used to study vibrational energy transfer are instead often based on approximations such as weak coupling or near equilibrium,^{24,25} which do not hold in the present case.

Our aim is to obtain meaningful insights in the intramolecular vibrational distribution, following photoexcitation, in order to understand how the vibrational energy, concentrated at CI in a specific subset of vibrational modes, is partitioned among the whole vibrational states, until reaching a pseudo-equilibrium state. Besides being directly relevant for Ura photophysics in the gas phase,³⁰ including the photodissociation processes,³¹ this study represents also a first step towards the study of VC in solution, since it would shed light on the intramolecular vibrational process occurring in Ura and on the vibrational mode more likely to communicate with solvent molecules.

Independently of VC, furthermore, the study of nucleobases excited state decay has recently aroused a lot of interest, because of the biological implication of the interaction between UV radiation and DNA.³²⁻³⁴

2 Computational details

The electronic structure calculations employed the PBE0 functional, a parameter-free hybrid functional, where the amount of exact exchange has been determined in order to fulfill a number of physical conditions, without resorting to any fitting procedure.³⁵ Despite the absence of adjustable parameters, besides providing a reliable description of the ground state properties of several classes of compounds, TD-PBE0 results have shown an overall degree of accuracy comparable with that of the best last generation functionals, in the description of both bright and dark excitations, and both valence and Rydberg states.³⁶ Furthermore, the vibrational analysis performed on the ground of PBE0/TD-PBE0 results (excited state minima geometry and vibrational frequencies) turned out to be in remarkable agreement with the experimental indications for several classes of compounds.³⁷ For what concerns nucleobases, PBE0 has already provided a very accurate description of their bright states, providing vertical excitation and emission energies within ~ 0.15 eV the corresponding experimental absorption maxima.³⁸ In particular, for Ura in the gas phase, PBE0 results are very close to those obtained at the CCSD(T) and CASPT2 level.^{39–46} In fact the $S_0 \rightarrow S\pi$ vertical excitation energy computed at the PBE0/6-31G(d)//TD-PBE0/6-311+G(2d,2p) level is 5.26 eV, to be compared with the 5.25 eV value obtained at the CR-EOM-CCSD(T)/aug-cc-pVTZ level.⁴⁶ Our simulations will exploit the cost-effective 6-31G(d) basis set. Previous studies have indeed shown that while TD-PBE0/6-31G(d) is not expected to provide accurate and 'converged' (with respect to the size of the basis set) excitation energies, it gives reliable equilibrium geometries and allows a fairly accurate vibrational analysis, as shown by the computed IR spectra of a set of semirigid molecules⁴⁷ and by the general accuracy of the computed vibrationally resolved absorption spectra.³⁷

ADMP simulations. We have performed 10 independent ADMP (Atomic Density Matrix Propagation) simulation runs starting from the $CI_{0\pi}$ (labeled as CI0) and 10 starting from the ground state minimum (labeled as FC4)

with a nuclear kinetic energy of 0 eV and 4 eV, respectively. To obtain 10 distinguishable CI0 trajectories, the initial kinetic energy was set to 0.000001 Hartree and randomly distributed among the 36 Cartesian coordinates of the system. All the simulations were performed in the micro canonical ensemble with a time-step of 0.2 fs over an overall period of 10 ps. The locally developed code VAMD⁴⁸ (Vibrational Analysis from Molecular Dynamics trajectories) was used to obtain the evolution of the most significant geometry shift as well as the picture of the intramolecular vibrational energy redistribution during the process. Concerning the last point, we recall⁴⁹ that the normal modes (v) of any molecular systems are the eigenvectors (K_{ij}^v) of the covariance matrix of mass-weighted velocities \mathbf{K} with elements:

$$K_{ij} = \frac{1}{2} \langle \sqrt{(m_i m_j)} v_i v_j \rangle \quad [i, j = 1, \dots, 3N] \quad (1)$$

N , m , v_i being the the number of the atoms, the masses and the atomic velocities, respectively. The eigenvalues of $\mathbf{K}(\lambda_i^v)$ represent the average kinetic energy in each vibrational mode i along the selected period of simulation. Please note that these vibrational modes are anharmonic in nature.^{48,50} The anharmonic effects, providing the couplings between the different vibrational modes, are expected to play a relevant role in the IVR process.

The vibrational modes (eigenvectors of \mathbf{K}) at the $\text{CI}_{0\pi}$ point, being quite different from those of the ground state, are considered as time dependent ($K_{ij}^v(t)$). The covariance matrix \mathbf{K} was then re-evaluated at each time step of the simulation (t_n) by considering the set of points that fulfill the condition $t_n \pm \Delta t_n$, with $\Delta t_n = 0.2 \times 100$ fs, (or $t_n \pm \Delta t_n \in [0, 40]$ fs, if $t_n < 20$ fs).

The set of time dependent kinetic energies of each normal mode ($T^v(t)$) was then evaluated from the projection of the atomic velocities on each time dependent eigenvector ($K_{ij}^v(t)$).

In order to include the effect of the kinetic energy gained in the motion from the FC point to the CI, we have also performed ten 10-ps long simulations starting from the $\text{CI}_{0\pi}$ structure, with 1 eV of kinetic energy randomly distributed among the different vibrational modes (CI1 simulations).

All electronic structure calculations have been performed by using the Gaussian09 package.⁵¹

3 Results

3.1 A description of the Ura decay

Before analyzing our results, it is important to concisely review the most important features of the lowest energy excited states in Ura. Experiments reveal the presence of a strong absorption band at ~ 4.8 - 5.0 eV (depending on the solvent),^{32,39} and computations ascribe this feature to a $\pi\pi^*$ transition (hereafter $S\pi$), which mainly corresponds to an HOMO \rightarrow LUMO excitation.³⁹⁻⁴⁶ Different computational methods unanimously predict that $S\pi$ is not the lowest energy excited state in the FC region: an underlying dark state is predicted, with $n\pi^*$ character (hereafter S_n), which mainly arises from the excitation of an electron from the Lone Pair (HOMO-1) of the C₄-O₈ carbonyl group (see Figure 1) to the π^* LUMO.³⁹⁻⁴⁶ The degree of the involvement of S_n in the Ura photoactivated dynamics is still a very controversial issue,^{39,40,45} falling outside the focus of the present study, which instead deals with the radiationless $S\pi\rightarrow S_0$ decay.

TD-PBE0/6-311+G(2d,2p) geometry optimizations show that a planar stationary point is present on S_π (S_π -min^{pla*}), exhibiting a low imaginary frequency, at $-i220$ cm⁻¹, corresponding to the out of plane motion of H₆ and to an out of plane deformation of the pyrimidine ring, involving especially C₆ atom. The most significant geometry shift in S_π -min^{pla*} with respect to the FC structure involves the C₅C₆ bond length that increases by ~ 0.1 Å. The C₄O₈ bond length increases by only 0.02 Å, ruling out any significant involvement of the carbonyl π bond. The passage through a pseudo-planar plateau, is also suggested by Resonance Raman experiments on Ura in solution, indicating that the most intense bands correspond to in-plane stretching and bending.⁵²

According to our previous studies in solution, on the other hand, both in acetonitrile and in water a 'real' non-planar minimum is present ($S\pi$ -min),

where the ring adopts a boat-like conformation: N₃ and C₆ are out of the plane defined by N₁, C₂, C₄, and C₅, and undergo partial pyramidalization, with C₆-H₆ and N₃-H₃ bonds out of the average molecular plane).^{39,40}

It has not been possible to locate the non-planar minimum in the gas phase, due to the presence of the close-lying S_n state (destabilized relative to S_π in polar solvents), since geometry optimizations decay to S_n. In any case, in solution the S_π-min is separated by a negligibly small energy barrier (< 100 cm⁻¹) from the crossing region with S₀, suggesting fast radiationless decay to S₀.⁴⁰

CASSCF/CASPT2 calculations in the gas phase provide a similar picture to that obtained at the TD-DFT level.^{40,43a} CASSCF(14,10)/6-31G(d) geometry optimization of S_π leads to a pseudoplanar minimum, where only H₆ is out of the plane of the ring, that however disappears at the MS-CASPT2 level. This latter method indicates instead a barrierless path leading from the FC point to an ethene-like CI with S₀ (CI_{0π}), characterized by pyramidalization of C₅ and by out-of-plane distortion of H₅. Another recent MS-CASPT2 study⁴¹, confirming the importance of a proper inclusion of dynamical correlation effects, predicts the existence of a minimum on S_π surface, exhibiting a boat-like conformation of the six-membered ring, similar to that found in solution at the PCM/TD-PBE0 level,³⁹ separated by a very small energy barrier from an ethene-like CI with S₀. A detailed discussion of the computational studies on the gas phase dynamics of Ura is outside the scope of the present paper and we refer to some very recent reviews for a more thorough analysis.⁴² For what concerns the aim of this study it suffices to say that there is general consensus on the existence of the ethene-like CI, firstly located by Matsika,⁴⁴ while the existence of a real minima on the S_π surface, and the height of the energy barrier separating them from CI_{0π} is still matter of debate.^{42,43,45} In any case, also the studies predicting the existence of such a minimum suggest that it is separated by rather small energy barrier from the conical intersection with S_n and S₀.⁴⁵ On the balance, the curves reported in Figure 2 should thus provide a qualitative reliable picture of the S_π PES.

For what concerns the time scale of the decay, gas phase time-resolved spectra provide slightly different time-constants depending on the experimental technique adopted, the excitation wave-length and the fit procedure adopted. The first pump-prob ionization experiments^{30a-c} suggest monoexponential decay with a time-constant of 2.4 ps. More recent studies, with a better time resolution, show instead bi or tri-exponential decay, with an ultrafast component (≤ 100 fs), namely 130 fs (photoelectron imaging spectroscopy and mass-selected ion spectroscopy experiments in Ar, pump wave length at 267 nm)^{30e}, < 50 fs (time-resolved photoelectron spectroscopy with pump wave length at 250 nm),^{30d} and 90 fs (strong field electron dissociation experiments)^{30f}. All these studies reveal also the presence of a component on the ps time scale (1.05-2.6 ps) and one of them^{30d} suggests a tri-exponential decay, with a third intermediate time constant = 530 fs. The interpretation of these time-constants lead to several deviating suggestions concerning the decay mechanism from the $S\pi$ stationary point. Firstly an indirect $S\pi \rightarrow S_n \rightarrow S_0$ path, secondly, a direct $S\pi \rightarrow S_0$ path, and finally the coexistence of these two latter paths were put forward as explanations.^{40,43,45} In any case there is consensus that on a ~ 1 ps time-scale a non-negligible part of the excited WavePacket (WP) has reached $CI_{0\pi}$ and it has passed on S_0 .

Since our reference structure for S_0 and all the vibrational analysis have been performed at the PBE0 level, it is important to obtain a PBE0 estimate of the $CI_{0\pi}$ structure, in order to avoid spurious results simply due to the difference of geometrical parameters provided by PBE0 and CASSCF. As a consequence, we choose a representative structure from the $S_0/S\pi$ crossing region individuated with the help of our previous study of the $S\pi$ PES in solution. The structure, see Figure 1, is similar to that located by CASSCF(8/8) calculations³⁹ and the $S_0/S\pi$ energy gap is only 0.1 eV at the TD-PBE0/6-31G(d) level and 0.04 eV at the TD-PBE0/6-311+G(2d,2p) level.

From the energetic point of view - referencing the S_0 minimum energy to 0 eV - the $S\pi$ energy at the FC point is predicted at 5.45 and 5.29 eV by TD-PBE0/6-31G(d) and TD-PBE0/6-311+G(2d,2p) calculations, respec-

tively. The $S\pi$ -min^{pla*} is calculated at 5.13 and 4.98 eV employing TD-PBE0/6-31G(d) and TD-PBE0/6-311+G(2d,2p), respectively. Finally, the $CI_{0\pi}$ $S\pi$ energy is found at 4.0 eV and that of S_0 at 3.96 eV according to TD-PBE0/6-311+G(2d,2p) calculations and at 4.12 eV and 4.0 eV (S_0) according to TD-PBE0/6-31G(d) calculations.

3.2 Analysis of the simulation

The starting point of our study is $CI_{0\pi}$. We shall thus focus on the system soon after its decay to S_0 , looking for an atomistic description of the IVR. As discussed in the previous section, the WP reaches the $CI_{0\pi}$ with a maximum of ~ 1 eV of excess kinetic energy (the difference between the energy of the pump pulse and that of the CI). Only a detailed quantum dynamical study of the WP dynamics, following photoexcitation, of its motion on the $S\pi$ PES, its possible interaction with Sn and, then, of the dynamics around the CI could provide insights on the amount of kinetic energy of the WP at the CI and on its distribution among the different vibrational degrees of freedom. Such a study is outside the scope of the present paper, focussed on the ground electronic state, and TD-DFT PES would not be suitable to study the dynamics in the proximity of the CI.⁵³ Instead we can envisage three limiting situations. In a first reference model, we assume that the WP arrives on S_0 at the $CI_{0\pi}$ with 0 kinetic energy, since it has lost at the CI all the excess energy coming from light absorption, for example due to the interaction with Sn or because it remains on the part of the WP still on the $S\pi$ surface. In a second scenario the initial state at $CI_{0\pi}$ has the excess kinetic energy of 1 eV randomly distributed that among the molecular degrees of freedom. In a final scenario, this excess energy is initially rather localized on what are most likely the most active coordinates in the $FC \rightarrow CI_{0\pi}$ transition.

In this study we shall mainly explore the first scenario; ten 10 ps independent simulations on S_0 (hereafter labeled as CI0 simulations) are performed starting from $CI_{0\pi}$ with 0 excess energy monitoring the redistribution of the potential energy among the different degrees of freedom during the path of

the WP towards the FC point. As for the second scenario, ten 5 ps simulations starting from the $CI_{0\pi}$ structure, with 1 eV of kinetic energy randomly distributed among the different vibrational modes (CI1 simulations) are performed. As discussed above, the study of the third scenario described above, in principle very interesting, requires the knowledge of the vibrational motions on the Excited state PES, before the WP has reached the CI, and of the behavior of the WP at $CI_{0\pi}$. Both tasks are beyond the aims of this study. On the other hand, in order to get some very preliminary insights on this scenario, we have performed a test simulation where 1 eV of kinetic energy is concentrated on a single, presumably important, vibrational degrees of freedom (see section 3.2.2.). Since we are dealing with an isolated system, the energy cannot be dissipated through intermolecular interactions; as a consequence our reference 'equilibrium' system would be that obtained by 10 independent ground state simulations starting from the S_0 minimum, with 4 eV of excess kinetic energy (FC4 simulations).

We shall start our analysis by examining how the geometry parameters change during our MD simulations, focussing mainly on the first ps of simulation, since it provides a more reliable base to get insights on the processes operating in solution. In the first hundreds of fs after the decay to the ground state, intramolecular vibrational redistribution is dominated by the couplings existing among uracil vibrational modes. On a longer time-scale the interaction with solute-solvent vibrations comes instead significantly into play, making an analysis focussed only on the solute vibrations less relevant. On the other hand, for some degrees of freedom we shall discuss the results for the entire simulation time (1-10 ps, the relevant plots are shown in the Supporting Information, SI); besides to providing the limit values of our simulations, they can be important to understand the IVR in the gas phase or in non-polar solvents.

3.2.1 Main geometry parameters

C₅-C₆ moiety Ura structure at $CI_{0\pi}$ is strongly distorted, and the most significant shifts with respect to FC concern the C₅-C₆ moiety: the C₅-C₆ bond

is elongated by 0.1 Å, being more similar to a single one; C₆ and, especially, C₅ are strongly pyramidalized, with the C₅ out of the average molecular plane and H₅ almost perpendicular to the latter (see Fig. 1). We can therefore expect that, once on S₀, C₅-C₆ moiety is that undergoing the most significant changes and the most of the kinetic energy is localized on this local mode. We therefore start our analysis with these degrees of freedom.

In the first hundreds of fs C₅-C₆ bond distance undergoes indeed a significant decrease: after 200 fs of simulation its average value decreases from 1.45 Å to 1.374 Å, and after 1 ps to 1.368 Å. This distance is already very close (see Fig. 3) to the average value found after 10 ps (the black circle at 1.365 Å), and only 0.007 Å larger than the average value found in FC4 simulations. After 10 ps the C₅-C₆ distance is 1.365 Å and this value is affected by the longer average distances found in the first ps of the simulation: the average distance in the last 2 ps is 1.364 Å and in the last ps 1.363 Å. By comparison, the corresponding average value in FC4 MD simulations is 1.359 Å. Analogously the RMSD in the first ps of the CI0 simulation is double (0.034 vs 0.017) than in the FC4 simulations, but already in the 1-3 ps range the CI0 and FC4 simulations exhibit rather similar RMSD values (0.0168).

The C₄-C₅-C₆ angle (see Figure in the SI) exhibits a behavior similar to that just described for the C₅-C₆ bond undergoing a very steep increase in the first 200 fs of the simulation, reaching quickly values ($\sim 118^\circ$) similar to that found after 10 ps (and in the FC4 simulations).

Figure 4 reports the variation of the main dihedral angle associated to the C₅ atom. Confirming the results discussed above, after 200 fs their average is already very close to 0°, as in the ground state minimum. Interestingly, C₅-C₆-N₁-C₂ dihedral that at the CI_{0π} is the most distorted is also the fastest to regain planarity, showing very small oscillations around the average value, at difference with C₅-C₄-N₃-C₂ dihedral angle, which shows noticeable oscillations up to 1 ps (actually up to 2.5 ps, see SI).

As discussed in in the SI, C₅-H₅ and C₆-H₆ bond lengths also quickly recover average values close to those found in the FC4 simulations.

C_6-N_1 bond distance (see SI), after an extremely sharp increase (from 1.33 Å up to 1.43 Å) in the first 200 fs (likely due to a flux of kinetic energy from C_5-C_6) mirrored by a very large RMSD (0.10), exhibits a slow decrease, with a similar RMSD than in FC4 simulation, but a slightly longer distance. In the last 2 ps the average C_6-N_1 distance is indeed 1.40 Å in the CI0 simulations and 1.39 in the FC4 ones. Analogously (see SI) the C_4-C_5 distance in the first 300 fs exhibits a sudden increase, due not only to the kinetic energy flowing from the C_5-C_6 bond but also to the intrinsic electronic features of the S_0 PES (the C_4-C_5 bond length is shorter at the CI, 1.432 Å, than in the S_0 minimum, 1.456 Å). However, within 1 ps its average value is very similar to that found in the last ps of the simulation (1.480 Å). This value is only slightly larger than that found in the last ps of the FC4 simulations (1.475), the two sets of simulations exhibiting very similar RMSD values (0.02 and 0.019, respectively) in this interval.

N3 moiety N_3-C_4 bond is one of the most active degrees of freedom during the simulation time (see Fig. 5). At the $CI_{0\pi}$ it is significantly elongated at 1.445 Å (in the S_0 minimum it is 1.40 Å), while N_3 undergoes partial pyramidalization. As expected, it shows a noticeable activity at the beginning of the simulation. In the first 200 fs it starts, on the average, decreasing. Its average value after the first 200 fs becomes indeed 1.43 Å, i.e. practically the same than that found in the FC4 simulation, as most of the kinetic energy has flown into other degrees of freedom. However, between 0.5 and 2 ps it shows a remarkable average lengthening, with a larger activity than in the FC4 simulations up to 10 ps. Its length average over 10 ps is ~ 1.442 Å, rather close to the starting value at the $CI_{0\pi}$ and almost 0.014 Å longer than the 10 ps average in the FC4 simulations. Interestingly, even in the last ps of the simulation the N_3-C_4 bond length is longer by ~ 0.01 Å in CI0 than in FC4 simulations, with a larger RMSD (0.026 vs 0.022).

C_2-N_3 exhibits a similar behavior to N_3-C_4 (see Fig. 5), but for a smaller activity at the beginning of the simulation, since its value at the $CI_{0\pi}$ is more similar to that of the S_0 minimum (it is smaller by ~ 0.015 Å). After 400 fs

its average value in CI0 and MD4 simulations is extremely similar (1.395 and 1.393 Å, respectively). Starting at 400-500 fs, we then observe a significant flow of kinetic energy, and the average bond length in CI0 simulations is higher than that issuing from FC4 simulations. In the 400 fs-1 ps range the average C₂-N₃ bond length is 1.406 Å, with an RMSD value significantly higher than in the corresponding interval in the FC4 simulations. In the last ps of the CI0 simulations the C₂-N₃ average length is 1.407 Å, more than 0.01 Å longer than in FC simulation, with a noticeably larger RMSD (0.025 Å vs 0.018 Å).

The flow towards NH stretchings, especially N₃-H₃ seems to start after some hundreds of fs but then it continuously increases. N₃-H₃, indeed, after a very sudden small increases in the first fs of the simulation (its length at the CI_{0π} is slightly shorter than in the FC) exhibits a first 'jump' between 200 fs and 800 fs, when it reaches an average value of 1.023 Å. It then keeps almost continuously increasing, for the entire simulation time. In the last ps of the simulation its average length is 1.03 Å, i.e. 0.02 longer than at the CI.

The C₂-N₃-C₄ behavior somewhat mirrors that of the N₃ bond lengths (see Fig. 6). In the first 300 fs of the simulation time it exhibits a sharp increase. This is not surprising since the C₂-N₃-C₄ is significantly smaller (~124.2°) than in the FC (~128.5°). However, after 300 fs it starts significantly decreasing and its average value after 2 ps is 125°. This 'decreasing' trend continues also for longer simulation time. The average value between 6 and 8 ps, just to make an example, is 124 °, i.e. smaller than at the CI. Interestingly also FC4 simulations predict a decrease of the C₂-N₃-C₄ angle, though much smaller than that found in CI0 simulation, indicating that an excess of energy can be 'trapped' in this moiety, undergoing pyramidalization.

A detailed description of the behavior of the remaining degrees of freedom can be found in the SI

CI1 simulations

Finally, we have checked how our picture would change in the case that the WP reaches the CI_{0π} without any energy dissipation, i.e. with one 1 eV of extra kinetic energy (labelled as CI1 simulations). As shown in the SI, all the

internal degrees of freedom exhibit the same qualitative evolution, whether the initial kinetic energy is 0 eV or 1 eV in excess, which reveals the same behavior of the vibrational cooling. The two sets of simulations also lead to very similar average values for all the Ura degrees of freedom, as shown in Table 1, where it is reported the average of the absolute differences between the values observed for 0 eV of Kinetic Energy (KE) excess and 1 eV for KE excess, for 3 different regimes of the process: [0-200] fs, [200-1000] fs, [1000-5000] fs. However, some slight differences are observed that can reveal in which internal coordinates the kinetic energy excess is located, meaning that these internal coordinates are particularly involved in the IVR process. The excess is first located in the torsional motions of C₂-N₃, N₃-C₄ and C₄-C₅ bonds and also in the C₅-H₅, C₆-H₆, C₅-C₆, C₆-N₁, N₁-H₁ bonds. After about 200 fs the excess is rapidly spread in the opposite part of the system, to vest more particularly the C₂-N₃, N₃-C₄ and N₃-H₃ bonds. From the simulation of these two scenarii, a first observation of the kinetic energy propagation can be made. However this description can be improved from the evaluation of the kinetic energy flow along each time dependent eigenvector which is dealt within the next section.

3.2.2 Kinetic energy flow

Starting from the CI_{0π} point at 0 eV, the overall averaged kinetic energy oscillates between 1 and 3 eV, after some tents of fs. with an average period of 25 fs (see Figure 7, panel a). The amplitude of the oscillation slightly decreases after 500 fs and is found in the range 2±0.5 eV. Along the dynamics, the corresponding period becomes less defined and also decreases up to about 5-10 fs. The vibrational analysis reveals (see Figure 7, panel b) that more than 90% of the kinetic energy flow is partitioned on 12 normal modes (mode a to mode l) and decreases sharply to about 50% after 200 fs. Four of them (modes a,b,c,d) have a kinetic energy which can overtake 40% of the total flow during the process (see Figure 8). The analysis of the average atomic fluctuations along these modes reveals that they correspond to out-of-plane motions. Among these four modes, the mode a, and the mode d in a lesser

extent, flow during the process (see Figure 8). The mode a is a ring-puckering motion: this is a butterfly-like motion in which N_3, H_6 atoms and O_7, O_8 atoms move unsymmetrically. The mode d corresponds to the unsymmetrical out of plane motion of N_1 and C_5 atoms in which the C_6-H_6 bond tend to be stretched. From 200 to 600 fs after the decay, the remaining 50% of the kinetic energy flow is partitioned over the 18 remaining modes (mode m to mode ad).

Six of them (modes m,n,o,p,q,r) capture a non-negligible part of the kinetic energy flow. The modes m and n correspond to in plane motions, involving basically the atoms N_3-C_6 moving in-phase for the mode m, and the atoms N_1-C_4 moving 180° out-of-phase for the mode n. The average atomic fluctuations along the modes o,p,q,r clearly reveal the stretching motions of the two C_2-O_7 and C_4-O_8 bonds (modes o,p) and of the two NH bonds (modes q,r). These are the modes from which the kinetic energy can be released outside the molecule.

Between 600 fs and 1 ps, the partition of the kinetic energy among the different vibrational modes starts equilibrating, not exhibiting the large differences just described. On the other hand, it is clear that some modes still provide a larger contribution to the total kinetic energy. They correspond to some in-plane motions of the atoms belonging to the cycle (modes f,k,n) and also to in-plane motion in which the oxygen atoms are involved symmetrically (mode i) and un-symmetrically (mode s).

Now we examine the behavior of the IVR from the $CI_{0\pi}$ point by considering 1 eV of initial kinetic energy on the eigenvector that corresponds to ring-puckering motion (mode a) of Ura, to get some preliminary information on the third scenario discussed in the previous section. The total kinetic energy reaches 4 eV after 13 fs and draws a damped wave which oscillates after 250 fs in the range 2.5 ± 1 eV (see Figure 12 in the SI). Starting from 1 eV, the kinetic energy on the ring-puckering motion oscillates for a period of about 15-25 fs between 0 eV and a growing maximum amplitude that reaches 2.1 eV (50% of the total kinetic energy) after 60 fs and decreases up to 0 eV after 250 fs. This mode is then reactivated around 500 fs. to reach a maximum value of 0.5 eV. Four other modes involving the out of plane motion of H_5 and H_6 and

some in plane and out of plane motions of the ring are activated at the very beginning of the simulation (about 10 fs). Each of them absorbs about 1-1.5 eV from the mode a in the period 10-100 fs. These four modes are deactivated after 150-200 fs and are sparsely reactivated during the process for a very short period that does not exceed 10 fs. Then, most of the other modes start to be activated at 150 fs. They reach 0.5-1 eV of kinetic energy between 400 and 600 fs. We can conclude that concentrating all the excess of kinetic energy only on the ring-puckering motion does not influence profoundly the timescales to recover planarity.

4 Discussion

The analysis of the geometric parameters and of the kinetic energy during the simulations provides a clear and consistent picture of the processes ruling the IVR in uracil after the decay to S_0 through the $CI_{0\pi}$.

We can individuate three distinct time-regimes. The first corresponds to the time range 0-200 fs and it involves mainly the recovery of the average planarity, starting from the strongly distorted structure of uracil at the $CI_{0\pi}$. 50 % of the kinetic energy is indeed concentrated on only four vibrational modes, corresponding to out-of-plane motions. After ~ 250 fs the average values of all the dihedral angles have already reached a value close to 0° (or 180°), and then oscillate around this value for all the simulation. A first interesting point is that, although C_5-C_6 moiety exhibits the largest distortion from the planarity, after having reached the planarity it exhibits very small oscillations (see, for example, Figure 4), which is in line with the large stiffness of the C_5-C_6 double bond. C_5-C_6 bond average distances also decreases within 250 fs to a value close to that of a standard CC double bond.

At the same time, the intra-ring bond distances and angles start recovering the values they have at the S_0 minimum, while all the exo-cyclic ones (CO, NH, CH bond distances) increase. Interestingly, C_5-H_5 , N_1-C_6 and C_4-O_8 bonds show the largest elongation in the first 20 fs. C_5-H_5 , whose involvement can be

expected since this bond is strongly distorted at the $CI_{0\pi}$, however it recovers within 250 fs its initial value, whereas N_1-C_6 , at the $CI_{0\pi}$ significantly shorter than at the FC, after 180 fs starts decreasing. The C_4-O_8 bond length, instead, steadily increases in the first 250 fs, being the first 'recipient' of the kinetic energy flow coming from the C_5-C_6 bond, in line with the conjugation existing in the $C_5=C_6-C_4=O_8$ moiety. This result can be put in nice relation with the findings of transient IR experiments on Guanine in solution, indicating a significant involvement of the exocyclic CO bond in the vibrational cooling process.²³

The second time-regime can be identified in the 200-600 fs time range. After 250 fs the C_5-C_6 moiety has indeed almost reached its standard structure, i.e. similar to that issuing by FC4 simulations, and we witness a more substantial 'activation' of the degrees of freedom of the $C_2N_3C_4$ moiety: increase of the C_2-N_3 , N_3-C_4 , C_2-O_7 bond lengths and decrease of the $C_2-N_3-C_4$ bond angle, with non negligible oscillations of the associated dihedral angles, while the C_4-O_8 bond is still active. Finally, after 500~600 fs most of the average values are similar to that found after 10 ps. On the other hand, this does not mean that our system can be considered to have reached equilibrium. Our calculations show that some degrees of freedom keep evolving during the entire time of our simulations. In particular, the N_1-C_6 average bond length and the $C_2-N_3-C_4$ bond angle, after a strong increase in the first 200 fs, steadily decrease for 10 ps. The N_3-H_3 bond lengths, on the contrary, steadily increases, though the former degrees of freedom exhibit large variation in the first ps. The C_2-N_3 , C_2-O_7 and N_3-C_4 bond lengths strongly increase during the first ps, before getting close to their 'final' values (actually, the C_2-N_3 bond length exhibits a small but noticeable increases up to 10 ps).

The bond lengths of the CI_0 simulations are still different after 10 ps from that of FC4 simulation. It seems that the 'random' energy distribution put more energy on all the degrees of freedom (for example stretching NH and CH), while a complete redistribution of the energy localized in the $CI_{0\pi}$ in well specific modes could require more time.

The indications obtained by analyzing the variation of Ura geometrical parameters are fully confirmed by the analysis of the kinetic energy distribution during the simulation. In the first 200 fs of the simulation, more than 40% of the total kinetic energy is concentrated on only 4 modes, corresponding to out-of-plane motion of Ura, with predominant contribution from the C₅-C₆ moiety. In a subsequent time window, we then observe a significant activation of vibrational modes involving the carbonyl groups and the NH bonds.

In the end, our simulations thus provide a clear physical picture of the IVR process, showing a flow of kinetic energy from the C₅-C₆ moiety, more rigid, towards the bonds involving the N₃ atom, whose lengths increase and, at the same time, whose bond angle decreases. These findings suggest that the accumulation of kinetic energy on the C₂-N₃H₃-C₄ moiety leads to a larger pyramidalization of the N₃ atom, as in a Sp²→Sp³ partial re-hybridization. Similar trends, though quantitatively less significant, are obtained for the N₁ atom. At the same time significant quantity of energy accumulates on the C₂-O₇ and, especially, in the C₄-O₈ bonds. In other words, most of the vibrational energy shows a tendency to accumulate on the floppiest part of the molecule (the N₃ moiety) and the 'exocyclic' bonds. Interestingly, this energy does not flow back towards the C₅-C₆ moiety, whose behavior is rather quickly (within 1 ps) very similar to that predicted by the FC4 simulations.

Our findings are fully consistent with the experimental results concerning the solvent effect on vibrational cooling of nucleobases in solution,^{20–22} since the energy accumulated on the N₃-H and the carbonyl moiety can be effectively dissipated through solute-solvent hydrogen bonds. It seems that we do not observe a relevant flow of kinetic energy towards low-frequency motion as those involving dihedral angle variation (for example out of plane motion of the ring). Though the Ura planarity at the C₁₀π is strongly distorted, the planarity is very quickly recovered (with small RMSD). This finding would be also consistent with the involvement of high-frequency solute-solvent intermolecular modes in the cooling, low-frequency 'frictional' modes playing a less important role. Furthermore, our simulations show a significant activation of

CH and NH bonds, which can be related with the photodissociation of these bonds, following also one photon absorption.^{31a}

We have shown that this picture is valid also in one of the the other two limit situations we can have at the Conical Intersection (CoI). Adding one additional eV of kinetic energy randomly distributed on the different degrees of freedom do not affect the trends we have highlighted, but only increases the fluctuations of the systems. Furthermore, a very preliminary analysis of the third scenario we have mentioned, i.e. that a significant portion of the excess energy is localized on the vibrational degrees of freedom leading to the CoI, suggests that our picture holds also in this limit situation. The planarity is quickly recovered also when 1 eV of excess kinetic energy is concentrated on a single ring-puckering mode, and, in any case, most of the variations with respect to CI0 and CI1 simulations are found in the first the first hundreds of fs after the decay to S_0 . On this ground we expect that, as far as this test is representative, the first time-regime we described can last more than 200~250 fs, but then the system should proceed along the same lines we have proposed.

5 Conclusion

In the present study we have provided an atomistic description of the Intramolecular Vibrational Redistribution processes occurring on the ground state of Uracil, following UV excitation, after that WP has reached the ground state at the CI with the spectroscopic $\pi\pi^*$ excited state. To this aim we have performed a significant number (30) of ground state Ab Initio Molecular Dynamics simulation, by exploiting the accurate PBE0 functional, comparing the results obtained when starting from the $CI_{0\pi}$ point (with 0 or 1 eV of extra kinetic energy) and from the Franck-Condon point, with 4 eV of extra kinetic energy (corresponding to the Energy gap with $CI_{0\pi}$). The simulations have been performed for 10 ps a much longer period of that our analysis focus on (mainly the first ps). On this ground we think they provide a solid ground for discussing the most relevant redistribution processes in the gas phase.

The analysis of the variation of Ura structural parameters and of the redistribution of the total kinetic energy among the different vibrational modes provide an interesting picture of the IVR process, which can provide insights not only on the photo activated dynamics in the gas phase. We observe indeed a very fast (within 200 fs) and almost irreversible kinetic energy flow from the out-of-plane vibrational degrees of freedom involving the C₅-C₆ moiety, that most significantly distorted at the CI_{0π}, towards the exocyclic bonds, CO and NH groups, and then, towards the C₂-N₃-C₄ moiety. On the other hand, in the ground state C₅-C₆ bond is a 'stiff' degree of freedom, while the C₂-N₃-C₄ moiety is coupled with several medium- and low-energy vibrational modes that can effectively receive the kinetic energy flow, preventing its flow back to the C₅-C₆ moiety. We can hypothesize that a similar mechanism could be operative in several systems. CI are often reached by distorting a moiety that is rigid in the ground state and floppier in the excited state (e.g., in Ura, the C₅-C₆ bond), since this motion obviously leads to a large decrease of the energy gap between ground and excited states. Once the WP is back on the S₀ surface, we thus expect that most of the kinetic energy will flow towards the vibrational modes leading to recover from this distortion (in our case, restoring a planar C₅-C₆ double bond), but then it is all dissipated in the 'floppiest' part of the molecule, (in our case the N₃ moiety) and/or on the exocyclic part.

Besides its interest for the study of gas phase photo activated dynamics (for example, it could give insights on the preferred photo dissociative paths), our study can give some preliminary, but useful, hints on the Vibrational Cooling process in solution. Our picture is indeed fully consistent with the experiments showing that solute-solvent hydrogen bonds (involving NH and CO groups) play a significant role in the VC of several nucleobases and that the VC process in the closely related Thymine molecule is insensitive to the temperature.^{24,25}

Our analysis is based on a classical description of the nuclear motions, and thus we cannot properly describe quantum vibronic effects. On the other hand, although methods rooted in MultiConfigurational Time Depen-

dent Hartree (MCTDH) theory,⁵⁴ coupled to a hierarchical transformation of the hamiltonians,^{55,56} have hugely increased the range of applicability of Quantum Dynamical approaches, a full anharmonic treatment of a molecule as uracil is still very challenging. From the methodological point of view, our study thus provides encouraging indications on the usefulness of atomistic simulation to integrate phenomenological model for understanding complex processes as IVR and vibration cooling.

6 Acknowledgments

The authors thanks Falk Richter for careful reading of the manuscript and very useful suggestions. RI thanks MIUR (PRIN 2010-2011 prot. 2010ERFKXL) and PICS French program.

References

- [1] T Elsaesser and W Kaiser Vibrational and Vibronic Relaxation of Large Polyatomic Molecules in Liquids *Annu. Rev. Phys. Chem.*, 1991, **42**, 83-107.
- [2] J.C. Owrutsky , D. Raftery and R.M. Hochstrasser *Annu. Rev. Phys. Chem.*, 1994, **45**, 519-55. Vibrational relaxation dynamics in solutions.
- [3] E.T. Nibbering and T. Elsaesser *Chem. Rev.* , 2004, **104**, 1887-914. Ultrafast vibrational dynamics of hydrogen bonds in the condensed phase.
- [4] E.T. Nibbering, H. Fidder and E. Pines *Annu. Rev. Phys. Chem.*, 2005, **56**, 337-67. Ultrafast chemistry: using time-resolved vibrational spectroscopy for interrogation of structural dynamics.
- [5] M. Banno, K. Ohta, S. Yamaguchi, S. Hirai and K. Tominaga *Acc. Chem. Res.*, 2009, **42**, 1259-69. Vibrational dynamics of hydrogen-bonded complexes in solutions studied with ultrafast infrared pump-probe spectroscopy.
- [6] (a) Y Kimura, M. Fukuda, O. Kajimoto and M. Terazima *J. Chem. Phys.*, 2006, **125**, 194615. (b) S.A. Kovalenko R. Schanz, H. Hennig and N.P. Ernstring *J. Chem. Phys.* 2001, **115**, 3256. (c) V. Kozich, W. Werncke, A.I. Vodchits and J. Dreyer, *J. Chem. Phys.*, 2003, **118**, 1808. (d) T. Schrader, A. Sieg, F. Koller , W. Schreier, Q. An, W. Zinth and P. Gilch, *Chem. Phys. Lett.*, 2004, **392**, 358. (e) M. Li, J. Owrutsky, M. Sarisky, J.P. Culver, A. Yodh and R.M. Hochstrasser, *J. Chem. Phys.*, 1993, **98**, 5499.
- [7] R.M. Stratt and M. Maroncelli Nonreactive dynamics in solution: The emerging molecular view of solvation dynamics and vibrational relaxation. *J. Phys. Chem.* ,1996, **100**, 12981-12996.
- [8] D.J. Nesbitt and R.W. Field Vibrational energy flow in highly excited molecules: Role of intramolecular vibrational redistribution. *J. Phys. Chem.* ,1996, **100**, 12735-12756.

- [9] S.Albert, K.K.Albert, H.Hollenstein, C.Manca Tanner, and M.Quack in "Handbook of High Resolution Spectroscopy", M.Quack and F.Merkt (eds.) Vol. 1, p 117 (Wiley, 2011)
- [10] R.M. Hochstrasser Multidimensional ultrafast spectroscopy *Proc. Natl. Acad. Sci. U.S.A.*, 2007, **104**, 14190-14196
- [11] F. F Crim, Chemical dynamics of vibrationally excited molecules: Controlling reactions in gases and on surfaces *Proc. Natl. Acad. Sci. U.S.A.* 2008, **105**, 12654-12661
- [12] K. L. Reid Picosecond time-resolved photoelectron spectroscopy as a means of gaining insight into mechanisms of intramolecular vibrational energy redistribution in excited states *Int. Rev. Phys. Chem.*, 2008, **27**, 607-628.
- [13] a) O.K. Rice and H.C. Ramsperger, Theories of unimolecular gas reactions at low pressures. *J. Am. Chem. Soc.*, 1927, **49**, 1617-1629. b) L.S. Kassel, Studies in homogeneous gas reactions. I. *J. Phys. Chem.* 1928, **32**, 225-242. c) R.A. Marcus, Unimolecular dissociations and free radical recombination reactions. *J. Chem. Phys.*, 1952, **20**, 359-364.
- [14] H. Guo and B.Jiang The Sudden Vector Projection Model for Reactivity: Mode Specificity and Bond Selectivity Made Simple *Acc. Chem. Res.* 2014, **47**, 3679-3685
- [15] M. Gruebele and P.G. Wolynes Vibrational Energy Flow and Chemical Reactions *Acc. Chem. Res.*, 2004 **37**, 261
- [16] C.G. Elles and F.F. Crim Connecting chemical dynamics in gases and liquids. *Annu. Rev. Phys. Chem.* 2006, **57**, 273-302.
- [17] P.M. Felker and A.H. Zewail Ultrafast dynamics of IVR in molecules and reactions. In: J.M. Hollas and D.Phillips editors. *Jet Spectroscopy and Molecular Dynamics*. London: Blackie Academic; 1995. pp. 222-308.

- [18] Y. Yamada, Y. Katsumoto and T. Ebata *Phys. Chem. Chem. Phys.*, 2007, **9**, 1170-85. Picosecond IR-UV pump-probe spectroscopic study on the vibrational energy flow in isolated molecules and clusters.
- [19] Y. Yamada, N. Mikami, and T. Ebata *Proc. Natl. Acad. Sci. U.S.A.*, 2008, **105**, 12690-12695. Relaxation dynamics of NH stretching vibrations of 2-aminopyridine and its dimer in a supersonic beam
- [20] Y. Zhang, J. Chen and B. Kohler *J. Phys. Chem. A*, 2013, **117**, 6771-6780.
- [21] C.T. Middleton, B. Cohen and B. Kohler *Journal of Physical Chemistry A*, 2007, **111**, 10460-10467.
- [22] J.L. Pecourt, J. Peon and B. Kohler *J. Am. Chem. Soc.*, 2001, **123**, 10370-10378.
- [23] Y. Zhang, R. Improta, B. Kohler *Phys. Chem. Chem. Phys.*, 2014, **16**, 1487-99.
- [24] B.A. West, J. M. Womick and A.M. Moran *J. Phys. Chem. A*, 2013, **117**, 5865-5874.
- [25] B.A. West, J.M. Womick and A.M. Moran *J. Chem. Phys.*, 2011, **135**, 114505.
- [26] J. B. Nielsen, J. Thogersen, S. K. Jensen, S. B. Nielsen and S. R. Keiding, *Phys. Chem. Chem. Phys.*, 2011, **13**, 13821-13826.
- [27] M. K. Kuimova, J. Dyer, M. W. George, D. C. Grills, J. M. Kelly, P. Matousek, A. W. Parker, X. Z. Sun, M. Towrie and A. M. Whelan, *Chem. Commun.*, 2005, 1182-1184.
- [28] D. A. McGovern, S. Quinn, G. W. Doorley, A. M. Whelan, K. L. Ronayne, M. Towrie, A. W. Parker and J. M. Kelly, *Chem. Commun.*, 2007, 5158-5160.
- [29] Fisher, G. J.; Johns, H. E. In *Photochemistry and Photobiology of Nucleic Acids*; Wang, S. Y., Ed.; Academic Press: New York, 1976; Vol. 1, p 169.
- [30] (a) Y.-G. He, C.-Y. Wu and W. Kong, *J. Phys. Chem. A*, 2004, **108**, 943. (b) H. Kang, K. T. Lee, B. Jung, Y. J. Ko and S. K. Kim, *J. Am.*

- Chem. Soc.*, 2002, **124**, 12958. (c) Y.-G. He, C.-Y. Wu and W. Kong, *J. Phys. Chem. A*, 2003, **107**, 5145. (d) S. Ullrich, T. Schultz, M. Z. Zgierski and A. Stolow, *Phys. Chem. Chem. Phys.*, 2004, **6**, 2796. (e) C. Canuel, M. Mons, F. Piuzzi, B. Tardivel, I. Dimicoli and M. Elhanine *J. Chem. Phys.*, 2005, **122**, 074316. (f) S. Matsika, M. Spanner, M. Kotur and T.C. Weinacht *J. Phys. Chem. A*, 2013, **117**, 12796-12801.
- [31] (a) M. Schneider, C. Schon, I. Fischer, L. Rubio-Lago and T. Kitsopoulos *Phys. Chem. Chem. Phys.*, 2007, **9**, 6021-6026. (b) J.C. Marcum, A. Halevi and J.M. Weber *Phys. Chem. Chem. Phys.* 2009, **11**, 1740-1751.
- [32] (a) C.E. Crespo-Hernandez, B. Cohen, P.M. Hare and B. Kohler, *Chem. Rev.*, 2004, **104**, 1977-2020. (b) C. T. Middleton, K. de La Harpe, C. Su, U. K. Law, C. E. Crespo-Hernandez and B. Kohler, *Ann. Rev. Phys. Chem.*, 2009, **60**, 217-239;
- [33] T. Gustavsson, R. Improta and D. Markovitsi, *J. Phys. Chem. Lett.*, 2010, **1**, 2025-2030.
- [34] K. Kleinermanns, D. Nachtigallova and M.S. de Vries, *Int. Rev. Phys. Chem.*, 2013, **32**, 308-342.
- [35] (a) C. Adamo and V. Barone *J. Chem. Phys.*, 1999, **110**, 6158-6170. (b) M. Enzerhof and G.E. Scuseria *J. Chem. Phys.*, 1999, **110**, 5029-5036.
- [36] D. Jacquemin, E.A. Perpète, I. Ciofini and C. Adamo *Acc. Chem. Res.* **42**, 326-334 (2009)
- [37] (a) R. Improta, V. Barone and F. Santoro, *Angew. Chem., Int. Ed.*, 2007, **46**, 405-408; (b) R. Improta, V. Barone and F. Santoro *J. Phys. Chem. B*, 2007, **111**, 14080. (c) F. Santoro, R. Improta, A. Lami, J. Bloino and V. Barone *J. Chem. Phys.*, 2007, **126**, 084509.
- [38] R. Improta and V. Barone *Top. Curr. Chem.* 2015, **355**, 329-357.
- [39] (a) T. Gustavsson, A. Banyasz, E. Lazzarotto, D. Markovitsi, G. Scalmani, M.J. Frisch, V. Barone and R. Improta, *J. Am. Chem. Soc.*, 2006, **128**, 607. (b) F. Santoro, V. Barone, T. Gustavsson and R. Improta *J.*

- Am. Chem. Soc.*, 2006, **128**, 16312-16322. (c) R. Improta, A. Lami, V. Barone and F. Santoro *Int J. Quantum Chem.*, 2010, **110**, 624-636.
- [40] Y. Mercier, F. Santoro, M. Reguero, and R. Improta *J. Phys. Chem. B*, 2008, **112**, 10769-10772.
- [41] S. Yamazaki and T. Taketsugu *J. Phys. Chem. A* 2012, **116**, 491-503.
- [42] (a) A. Giussani, J. Segarra-Martí, D. I. Roca-Sanjuán and M. Merchán *Top. Curr. Chem.* 2015, **355**, 57-98; (b) S. Mai, M. Richter, P. Marquetand and L. González *Top. Curr. Chem.* 2015, **355**, 99-53
- [43] (a) M. Merchán, R. Gonzalez-Luque, T. Climent, L. Serrano-Andres, E. Rodriiguez, M. Reguero and D. Pelaez *J. Phys. Chem. B*, 2006, **110**, 26471. (b) X. Zhang and J. M. Herbert *J. Phys. Chem. B.*, 2014, **118**, 7806-7817.
- [44] S. Matsika, *J. Phys. Chem. A*, 2004, **108**, 7584
- [45] (a) D. Nachtigallová, A.J.A. Aquino, J.J. Szymczak, M. Barbatti, P. Hobza and H. Lischka *J. Phys. Chem. A*, 2011, **115**, 5247-5255 (b) H.R. Hudock, B.G. Levine, A.L. Thompson, H. Satzger, D. Townsend, N. Gador, S. Ullrich, A. Stolow and T.J. Martinez *J. Phys. Chem. A*, 2007, **111**, 8500. (c) R. Improta, V. Barone, A. Lami and F. Santoro *J. Phys. Chem. B.*, 2009, **113**, 14491-14503.
- [46] E. Epifanovsky, K. Kowalski, P.-D. Fan, M. Valiev, S. Matsika and A.I. Krylov *J. Phys. Chem. A*, 2008, **112**, 9983-9992.
- [47] P. Carbonniere, T. Lucca, C. Pouchan, N. Rega and V. Barone. *J. Comput. Chem.*, 2005, **26**, 384.
- [48] P. Carbonniere, A. Dargelos, I. Ciofini, C. Adamo and C. Pouchan *Phys. Chem. Chem. Phys.*, 2009, **11**, 4375-84.
- [49] A. Strachan *J. Chem. Phys.*, 2004, **120**, 1-4.
- [50] (a) N. Rega *Theor. Chem. Acc.* 2006, **116**, 347-354; (b) P. Carbonniere and C. Pouchan, *Int. J. Quantum Chem.* 2010, **110**, 578-585.

- [51] Gaussian 09, Revision A.2; Gaussian, Inc.: Wallingford, CT, 2009, M.J. Frisch et al.
- [52] (a) S. Yarasi, P. Brost and G.R. Loppnow, *J. Phys. Chem. A*, 2007, **111**, 5130-5135 (b) B. E. Billinghamurst, R. Yeung and G.R. Loppnow *J. Phys. Chem. A*, 2006, **110**, 6185-6191 (c) W.R. Peticolas and T. Rush III. *J. Comput. Chem.*, 1995, **16**, 1262
- [53] (a) B.G. Levine, C. Ko, J. Quenneville and T.J. Martnez *Mol. Phys.*, 2006, **104**, 1039 (b) F. Cordova, L. J. Doriol, A. Ipatov, M.E. Casida, C. Filippi and A. Vela *J. Chem. Phys.* 2007, **127**, 164111.
- [54] H.-D. Meyer, U. Manthe, and L.S. Cederbaum. *Chem.Phys.Lett.*, 1990, **165**, 73.
- [55] R. Martinazzo, K. H. Hughes, and I. Burghardt, in: *Advances in the Theory of Quantum Systems in Chemistry*, Eds. P. Hoggan et al., Progress in Theoretical Chemistry and Physics, 2011, **22**, Chapter 12.
- [56] D. Picconi, F.J. Avila Ferre, R. Improta, A. Lami, F. Santoro F. *Faraday Discussions* 2013, **163**, 223.

Table 1: Mean absolute difference (\AA or degrees) between the CI0 and CI1 simulations for Ura degrees of freedom in three different time interval

| Coordinate | 0- 200 fs | 200-1000 fs | 1000-5000 fs |
|--|-----------|-------------|--------------|
| N ₁ -C ₂ | 0,005 | 0,003 | 0,006 |
| C ₂ -N ₃ | 0,004 | 0,007 | 0,007 |
| N ₃ -C ₄ | 0,004 | 0,005 | 0,007 |
| C ₄ -C ₅ | 0,004 | 0,002 | 0,004 |
| C ₅ -C ₆ | 0,006 | 0,004 | 0,002 |
| C ₆ -N ₁ | 0,008 | 0,002 | 0,003 |
| N ₁ -H ₁ | 0,008 | 0,004 | 0,003 |
| C ₂ -O ₇ | 0,001 | 0,003 | 0,003 |
| N ₃ -H ₃ | 0,005 | 0,005 | 0,008 |
| C ₄ -O ₈ | 0,003 | 0,001 | 0,001 |
| C ₅ -H ₅ | 0,005 | 0,001 | 0,001 |
| C ₆ -H ₆ | 0,017 | 0,009 | 0,002 |
| N ₁ -C ₂ -N ₃ | 0,2 | 0,1 | 0,1 |
| C ₂ -N ₃ -C ₄ | 1,0 | 0,9 | 0,7 |
| N ₃ -C ₄ -C ₅ | 0,8 | 0,2 | 0,3 |
| C ₄ -C ₅ -C ₆ | 0,8 | 0,1 | 0,1 |
| C ₅ -C ₆ -N ₁ | 0,4 | 0,2 | 0,1 |
| C ₆ -N ₁ -C ₂ | 0,7 | 0,2 | 0,5 |
| N ₁ -C ₂ -N ₃ -C ₄ | 6,9 | 1,3 | 0,2 |
| C ₂ -N ₃ -C ₄ -C ₅ | 10,7 | 1,6 | 0,4 |
| N ₃ -C ₄ -C ₅ -C ₆ | 7,1 | 1,0 | 0,3 |
| C ₄ -C ₅ -C ₆ -N ₁ | 0,9 | 0,3 | 0,1 |
| C ₅ -C ₆ -N ₁ -C ₂ | 3,0 | 0,4 | 0,2 |
| C ₆ -N ₁ -C ₂ -N ₃ | 2,6 | 0,6 | 0,2 |

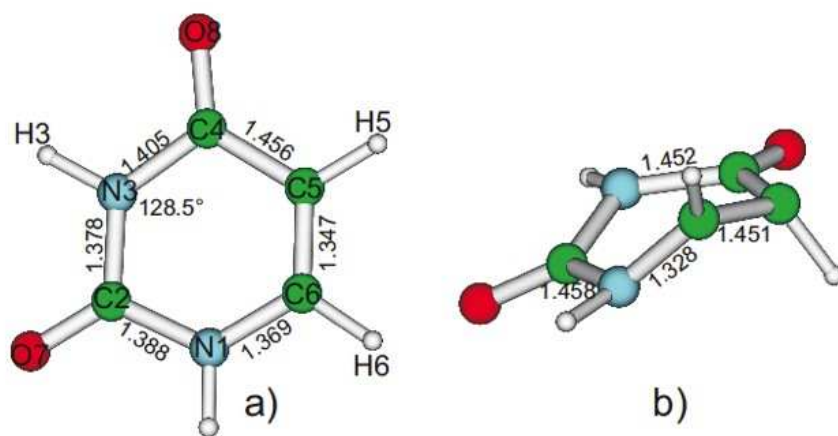


Figure 1: Schematic drawing, atom labeling, and selected bond distances (in Å) of uracil in FC point (S_0 minimum, a) and at the S_π/S_0 CI (b)

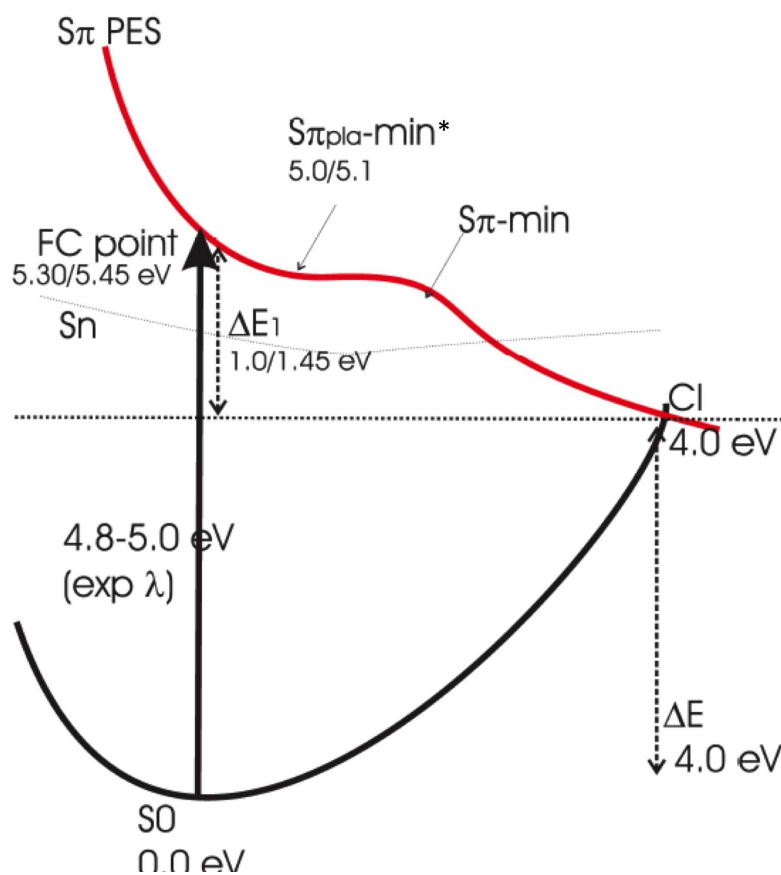


Figure 2: Schematic drawing of the Potential Energy Surfaces of the excited state involved in the Uracil photophysics

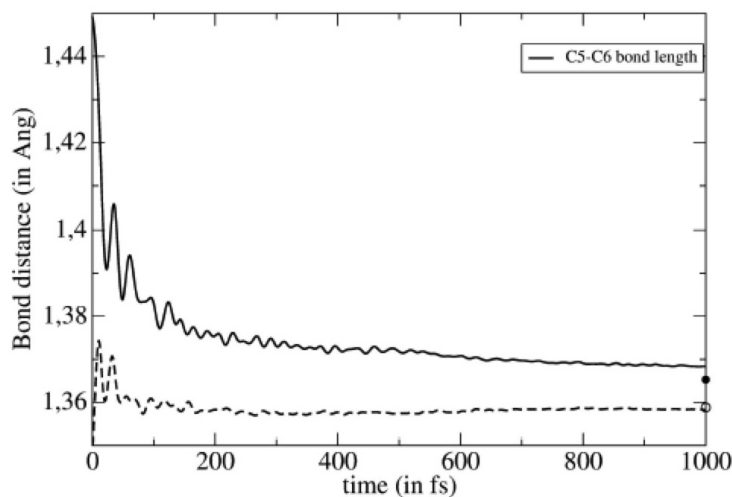


Figure 3: Variation of the average C5-C6 bond length according to the CI0 (continuous line) and FC4 (dashed lines) averaged simulations. The average value over the 0-10 ps averaged simulations is marked with a filled circle (CI0 simulations) or an empty circle (FC4 simulations)

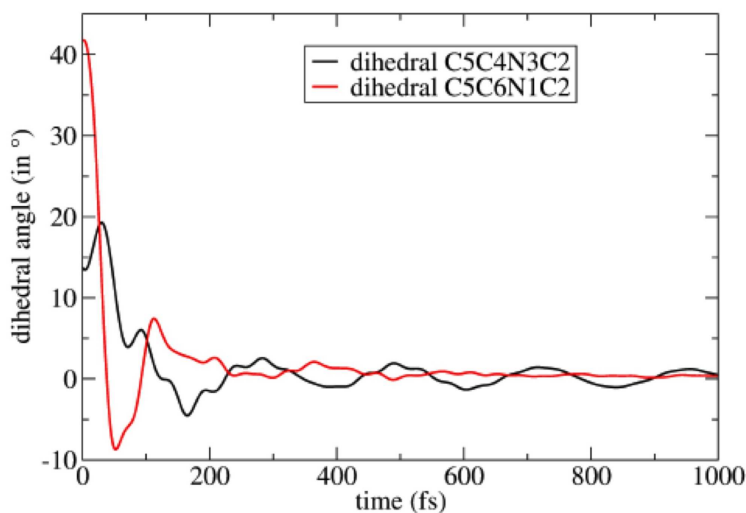


Figure 4: Variation of the average and C5-C4-N3-C2 (black) and C5-C6-N1-C2 (red) dihedral angles according to the CI0 averaged simulations. The average value over the 0-10 ps averaged simulations is marked with a filled circle (CI0 simulations) or an empty circle (FC4 simulations)

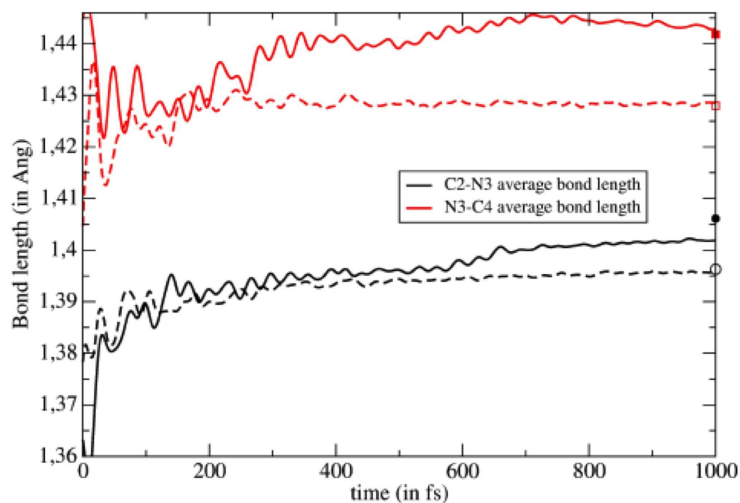


Figure 5: Variation of the average C2-N3 and N3-C4 bond lengths according to the CI0 (continuous line) and FC4 (dashed lines) averaged simulations. The average value over the 0-10 ps averaged simulations is marked with a filled circle (CI0 simulations) or an empty circle (FC4 simulations).

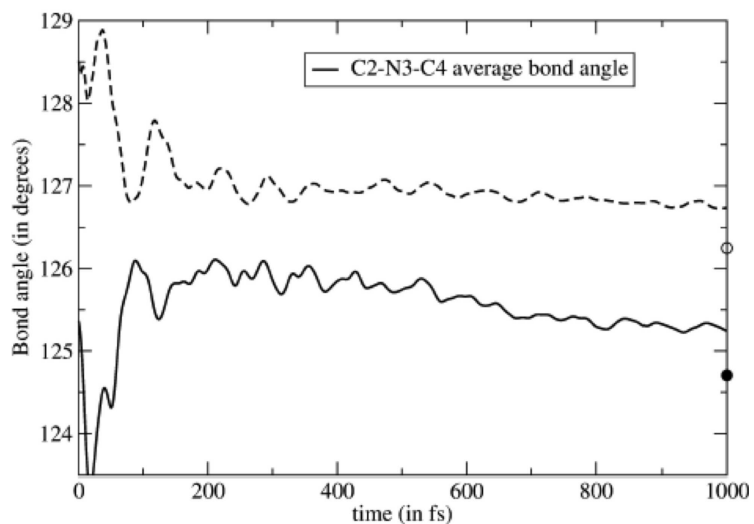


Figure 6: Variation of the average C2-N3-C4 bond angle according to the CI0 (continuous line) and FC4 (dashed lines) averaged simulations. The average value over the 0-10 ps averaged simulations is marked with a filled circle (CI0 simulations) or an empty circle (FC4 simulations)

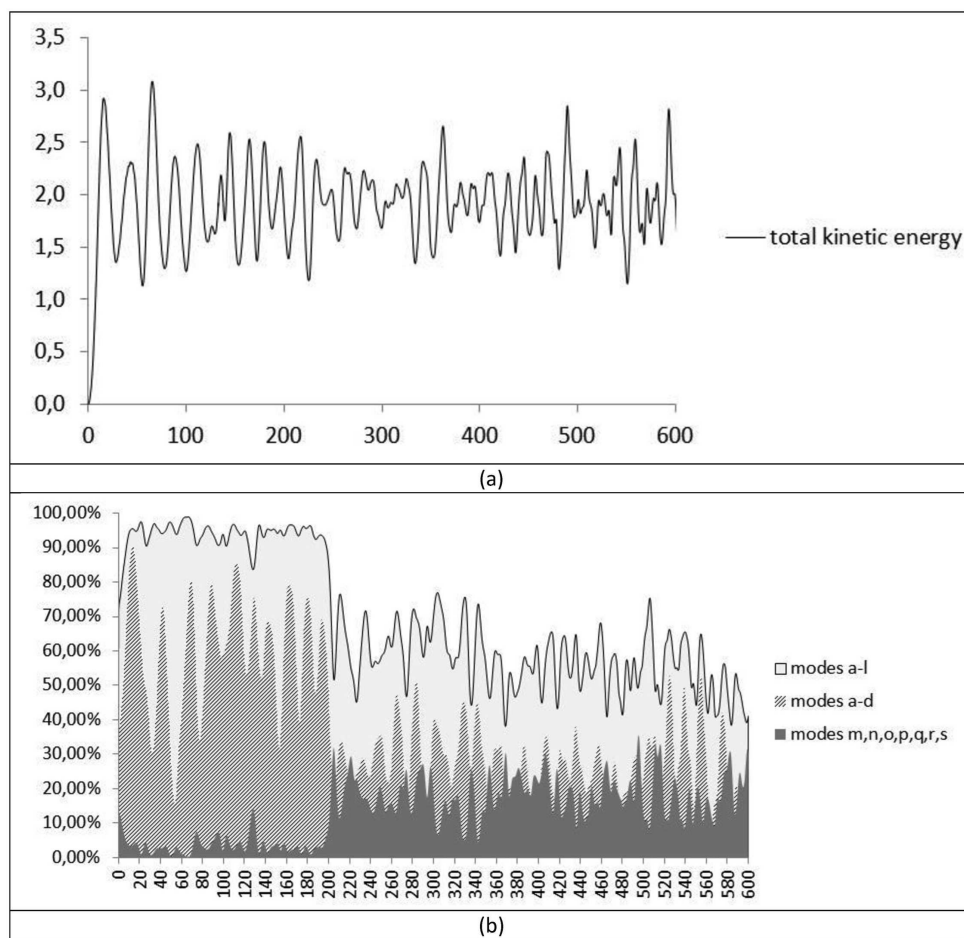


Figure 7: (a) Variation of the total kinetic energy averaged over 10 CI0 simulations in the interval 0-600 fs. (b) Decomposition of the total kinetic energy (averaged over 10 simulations) in the most relevant vibrational modes

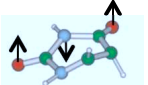
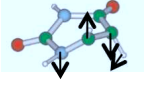
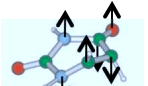
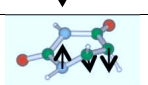
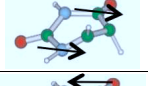
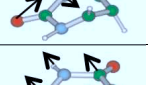
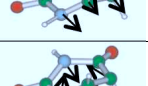
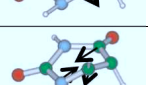
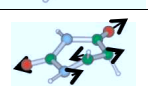
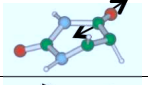
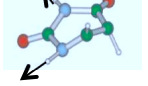
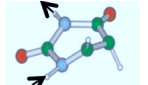
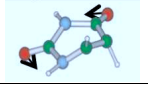
| Fluctuations at Cl ₀ | | 0-200 | 200-400 | 400-600 | 600-800 | 800-1000 |
|---------------------------------|---|------------------|-----------------|------------------|-----------------|-----------------|
| (a) |  | 24.8% (66.8%) | 6.5% (16.9%) | 2.6% (12.1%) | 4.1% (10.8%) | 1.6% (5.7%) |
| (b) |  | 14.9% (65.3%) | 9.4% (39.5%) | 12.4% (44.6%) | 3.3% (13.1%) | 6.7% (19.0%) |
| (c) |  | 12.0% (44.6%) | 9.5% (36.3%) | 6.7% (27.0%) | 7.6% (19.4%) | 3.6% (20.7%) |
| (d) |  | 7.8% (44.5%) | 3.0% (10.6%) | 4.6% (12.9%) | 3.7% (13.6%) | 2.8% (12.1%) |
| (f) |  | 6.0% (36.1%) | 5.7% (18.6%) | 3.8% (13.2%) | 4.4% (14.9%) | 4.4% (19.2%) |
| (i) |  | 4.0% (20.8%) | 3.9% (15.0%) | 3.6% (13.5%) | 3.8% (13.7%) | 5.3% (18.9%) |
| (k) |  | 2.2% (13.1%) | 2.3% (12.0%) | 3.9% (18.5%) | 3.0% (8.5%) | 4.5% (19.0%) |
| (m) |  | 1.6% (11.4%) | 3.8% (21.9%) | 2.5% (11.1%) | 4.0% (20.9%) | 3.2% (15.4%) |
| (n) |  | 1.4% (6.4%) | 4.8% (22.5%) | 3.9% (18.7%) | 4.2% (18.0%) | 5.0% (21.2%) |
| (o) |  | 0.4% (6.3%) | 2.6% (8.9%) | 3.1% (12.5%) | 2.5% (8.6%) | 3.1% (10.0%) |
| (p) |  | 0.3% (2.6%) | 3.0% (13.1%) | 2.7% (9.5%) | 3.4% (11.1%) | 2.9% (11.3%) |
| (q) |  | 0.0% (8.5%) | 1.6% (8.1%) | 3.2% (17.3%) | 3.6% (10.1%) | 2.4% (9.6%) |
| (r) |  | 0.0% (1.6%) | 2.7% (17.4%) | 3.3% (12.5%) | 3.0% (13.5%) | 2.9% (11.8%) |
| (s) |  | 0.0% (1.6%) | 0.4% (2.5%) | 1.1% (5.1%) | 3.3% (11.4%) | 5.0% (20.4%) |

Figure 8: Schematic description of some of the vibrational modes more involved in the vibrational relaxation process, and their average percentual contribution to the total kinetic energy in different time-ranges (the maximal contribution is given in parenthesis).